


Transport anisotropy and electron correlations in the layered molecular compounds $Z[\text{Pd}(\text{dmit})_2]_2$ ($Z = \text{Me}_4\text{N}, \text{Et}_2\text{Me}_2\text{As}, \text{EtMe}_3\text{P}$) with different interlayer coupling

Yasuhiro Shimizu^{1,2} and Reizo Kato¹¹*Condensed Molecular Material Lab., RIKEN, Wako, Saitama, 351-0198, Japan*²*Department of Physics, Graduate School of Science, Nagoya University, Furo-cho, Chikusa-ku, Nagoya 464-8602, Japan*
 (Received 22 November 2017; revised manuscript received 12 February 2018; published 5 March 2018)

In-plane resistivity ρ_{\parallel} and out-of-plane resistivity ρ_{\perp} were investigated across the pressure-induced Mott transition in molecular Mott insulators $Z[\text{Pd}(\text{dmit})_2]_2$ ($Z = \text{Et}_2\text{Me}_2\text{As}, \text{Me}_4\text{N}$, and EtMe_3P) having a triangular lattice. All three compounds exhibit superconducting transition with $T_c = 5.5\text{--}7.0$ K in the metallic phase near the Mott insulating phase. For the β' - $\text{Et}_2\text{Me}_2\text{As}$ salt, the anisotropy $\rho_{\perp}/\rho_{\parallel}$ exceeds 10^3 at low temperatures, indicating a highly two-dimensional electronic state with incoherent interlayer hopping. The β - Me_4N salt has a smaller $\rho_{\perp}/\rho_{\parallel}$ exhibiting a weak interlayer coupling. The resistivity is dominated by electron-electron scattering in the metallic state for these two compounds, as expected in a correlated Fermi liquid. On the other hand, the EtMe_3P salt with a valence bond order state becomes a nearly three-dimensional metal across the Mott transition, in which the electron correlation is strongly suppressed. Instead, the electron-phonon scattering plays a significant role in the resistivity. The different interlayer coherence is quantitatively explained by the calculated interlayer transfer integrals between $\text{Pd}(\text{dmit})_2$ molecules. These results suggest that the dimensionality governs the nature of electron correlations in the Fermi liquid state.

DOI: [10.1103/PhysRevB.97.125107](https://doi.org/10.1103/PhysRevB.97.125107)

I. INTRODUCTION

Dimensionality is one of the key factors that dominate phase transitions and electron correlations in many body systems. Quasi-two-dimensional (quasi-2D) electron systems including cuprate and organic compounds have provided many emergent phenomena such as unconventional Cooper pairing and non-Fermi liquid behavior. The 2D confinement of conducting electrons, which is manifested as, for example, the incoherent interlayer transport, results in heavily dressed quasiparticles beyond the Fermi liquid regime [1–7]. Layered organic conductors, such as κ -(ET)₂ X [$\text{ET} = \text{bis}(\text{ethylenedithio})\text{tetrathiafulvalene}$, X : anions], have been investigated as the quasi-2D Mott-Hubbard system on a frustrated triangular lattice [8,9]. The unconventional criticality of the pressure-driven Mott transition likely belongs to 2D universality [10,11], whereas the interlayer transport is coherent in a low-temperature metallic state, as observed in the angle dependence of magnetoresistance [12,13]. Systematic studies on ideal 2D and three-dimensional (3D) materials are required for understanding the Mott transition and superconductivity in strongly correlated systems.

A series of anion radical salts $Z[\text{Pd}(\text{dmit})_2]_2$ ($\text{dmit} = 1,3\text{-dithiole-2-thione-4,5-dithiolate}$, $Z = \text{monovalent cations}$) serve other triangular lattice Mott-Hubbard systems having charge and orbital degrees of freedom. The Mott insulating phases have various magnetic ground states such as Néel order, spin liquid, and nonmagnetic charge order, as a function of the transfer anisotropy t'/t in the triangular lattice of $\text{Pd}(\text{dmit})_2$ dimers (Fig. 1) in the conducting layer [14,15]. Moreover, the terminal S atoms on the $\text{Pd}(\text{dmit})_2$ molecule possess a high electron density near the Fermi level, which potentially gives rise to 3D coupling through the S-S contacts along the inter-

planar direction [14–16]. However, the dimensionality of the electronic states has not been investigated for $Z[\text{Pd}(\text{dmit})_2]_2$.

Here we focus on the anisotropy of electronic transport properties of $Z[\text{Pd}(\text{dmit})_2]_2$ with different packing patterns, called the β' , β , and EtMe_3P types ($\text{Et} = \text{C}_2\text{H}_5$ -, $\text{Me} = \text{CH}_3$ -), as shown in Fig. 1. The β' and β systems possess a monoclinic $C2/c$ lattice with a solid-crossing column structure, where $\text{Pd}(\text{dmit})_2$ molecules stack along the $a - b$ and $a + b$ axes in two crystallographically equivalent layers [14]. Each $\text{Pd}(\text{dmit})_2$ layer consists of a triangular lattice of $\text{Pd}(\text{dmit})_2$ dimers with approximately two kinds of interdimer transfers, t and t' . Most of $Z[\text{Pd}(\text{dmit})_2]_2$ including $Z = \text{Et}_2\text{Me}_2\text{As}$ and EtMe_3Sb belong to the β' type. With increasing t'/t toward unity, the geometrical frustration suppresses the Néel order temperature T_N [17–19]. For instance, T_N is 18 K for the $\text{Et}_2\text{Me}_2\text{As}$ salt ($t'/t = 0.87$) [15] and totally suppressed for the EtMe_3Sb salt with $t'/t = 0.91$ [20]. A nonmagnetic charge order state appears for the $\text{Et}_2\text{Me}_2\text{Sb}$ salt with $t'/t = 1.01$ because of the molecular orbital instability [21,22]. The β -type compounds with a slightly different cation location have lower Néel temperatures than the β' type; for example, $T_N = 12$ K for the Me_4N salt ($t'/t = 0.83$) [23]. $\text{EtMe}_3\text{P}[\text{Pd}(\text{dmit})_2]_2$ (monoclinic $P2_1/m$, $t'/t = 1.05$) has a parallel column structure with one stacking direction along the c axis [24], as shown in Fig. 1(c). A valence bond order (VBO) occurs through a spin $S = 1/2$ dimerization along the stacking direction at 25 K [25]. The thermal and field-driven Mott transitions occur at the critical pressure $P_c \sim 0.4$ GPa [26].

In this paper, we report the in-plane resistivity ρ_{\parallel} and the out-of-plane resistivity ρ_{\perp} on β - $\text{Me}_4\text{N}[\text{Pd}(\text{dmit})_2]_2$, β' - $\text{Et}_2\text{Me}_2\text{As}[\text{Pd}(\text{dmit})_2]_2$, and $\text{EtMe}_3\text{P}[\text{Pd}(\text{dmit})_2]_2$ (hereafter denoted as Me_4N , $\text{Et}_2\text{Me}_2\text{As}$, and EtMe_3P , respectively) that demonstrate the different interlayer coupling. We construct

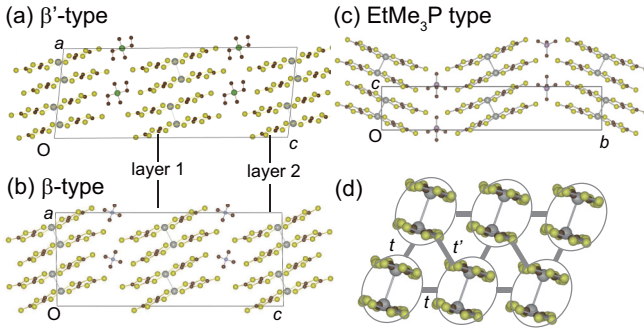


FIG. 1. Crystal structures of (a) β' - $\text{Et}_2\text{Me}_2\text{As}[\text{Pd}(\text{dmit})_2]_2$, (b) β - $\text{Me}_4\text{N}[\text{Pd}(\text{dmit})_2]_2$, and (c) $\text{EtMe}_3\text{P}[\text{Pd}(\text{dmit})_2]_2$, viewed from the b axis for (a) and (b), and from the a axis for (c). Cation locations are different between the β' and β structures. (d) Triangular lattice of the $\text{Pd}(\text{dmit})_2$ dimer with interdimer transfer integrals t and t' in the conducting layer.

the pressure-temperature phase diagram of $\text{Et}_2\text{Me}_2\text{As}$ and revise those of Me_4N and EtMe_3P beyond the previous reports [23,26]. We show that the electron correlation in the metallic state strongly depends on the confinement of electrons in the conducting layers. The variety of the interlayer coupling can be characteristic to the series of compounds.

II. EXPERIMENT

Single crystals of $Z[\text{Pd}(\text{dmit})_2]_2$ ($Z = \text{Me}_4\text{N}, \text{Et}_2\text{Me}_2\text{As}, \text{EtMe}_3\text{P}$) were prepared by aerial oxidation of $Z_2[\text{Pd}(\text{dmit})_2]$ in acetone containing acetic acid [15]. The typical sample size was $0.5 \times 0.5 \times 0.1 \text{ mm}^3$. ρ_{\parallel} and ρ_{\perp} were measured using a six-probe dc method. The contact arrangement is shown in Fig. 2(c). The Au leads were attached by carbon paste. The distance of the in-plane voltage probes (V_{\parallel}) were $\sim 0.2 \text{ mm}$ in Fig. 2(c). The current probes for ρ_{\parallel} measurements were attached to the sides of the crystal. We checked that ρ_{\perp} is independent of the contact positions by changing the voltage and current probes. The resistivity data were taken for two samples independently on each $\text{Pd}(\text{dmit})_2$ salt, which were quantitatively reproducible. The hydrostatic pressure was applied by using a BeCu-NiCrAl clamp cell and Daphne 7373 oil and monitored with the resistivity of a manganin wire at room temperature. The applied pressure is known to decrease because of the thermal contraction and solidification of the oil by 0.15–0.17 GPa at low temperatures [27]. The pressure values described below are those monitored at room temperature.

III. EXPERIMENTAL RESULTS

A. β' - $\text{Et}_2\text{Me}_2\text{As}[\text{Pd}(\text{dmit})_2]_2$

Figure 2(a) shows the temperature dependence of ρ_{\parallel} for $\text{Et}_2\text{Me}_2\text{As}$. On the Mott insulating phase at 0.3 GPa, ρ_{\parallel} exhibits an exponential increase with an activation gap of 45 meV at 100 K. With increasing pressure, ρ_{\parallel} becomes metallic and shows an upturn due to the metal-insulator crossover. The crossover temperature T_{MI} defined by the resistivity minimum is reduced at higher pressures, and the crossover sharpens toward the critical pressure $P_c \sim 0.7 \text{ GPa}$. Because T_{MI} is abruptly suppressed in a narrow pressure range

of 0.6–0.7 GPa, a slight pressure inhomogeneity in the sample may produce a fraction of metallic domains just below P_c . Above P_c , ρ_{\parallel} becomes metallic down to low temperatures. The superconducting transition is observed at $T_c = 5.5 \text{ K}$ for 0.71 GPa and is suppressed with pressure. In the metallic state, ρ_{\parallel} is well below the upper limit of the Boltzmann transport, called the Ioffe-Regel limit $\rho_{\text{IR}} = 3\hbar a/e^2 \sim 3 \text{ m}\Omega\text{cm}$ [28], corroborating the Fermi liquid regime and the negligible admixture of the ρ_{\perp} component.

The interlayer resistivity ρ_{\perp} is an order of magnitude larger than ρ_{\parallel} at 300 K [Fig. 2(b)]. It remains semiconducting with increasing pressure to 0.71 GPa; however, ρ_{\parallel} becomes metallic down to low temperatures. Even above 0.76 GPa, ρ_{\perp} remains nearly independent of temperature [Fig. 2(e)], indicating the incoherent interlayer transport in sharp contrast to ρ_{\parallel} . The 2D confinement is clearer when we plot the resistivity anisotropy $\rho_{\perp}/\rho_{\parallel}$ against temperature T , as shown in Fig. 2(c). $\rho_{\perp}/\rho_{\parallel}$ strongly depends on temperature with a maximum near T_{MI} . In the metallic region above 0.68 GPa, $\rho_{\perp}/\rho_{\parallel}$ continues to increase down to low temperatures and reaches 3×10^3 at 10 K. Thus, $\text{Et}_2\text{Me}_2\text{As}$ is well regarded as an ideal 2D Mott-Hubbard system.

The nature of quasiparticles in the metallic state can be featured by ρ_{\parallel} at low temperatures. ρ_{\parallel} is plotted against T^2 in Fig. 2(d). The good linearity below 20 K shows that ρ_{\parallel} follows a relation $\rho_{\parallel} = \rho_0 + A_{\parallel}T^2$ with constants ρ_0 and A_{\parallel} , characteristic to a Fermi liquid metal with electron-electron scattering. The T^2 coefficient A_{\parallel} is evaluated as 1.8–2.1 $\mu\Omega\text{cm}/\text{K}^2$, which is enhanced by an order of magnitude compared to weakly correlated metals such as β -(ET) $_2\text{I}_3$ [29], and unusually insensitive to pressure. On the other hand, ρ_{\perp} does not show the T^2 behavior but maintains high at values exceeding ρ_{IR} [Fig. 2(e)]. Therefore, the superconducting transition for ρ_{\perp} should occur through the intrinsic Josephson tunneling effect, as known in high- T_c cuprate superconductors [30].

These results are summarized in the pressure-temperature (P - T) phase diagram in Fig. 2(f). The phase boundary between the insulating and metallic phases is defined in the previous discussion. Although we have not identified the resistivity jump and hysteresis down to 20 K, the phase boundary between the antiferromagnetic insulator and superconducting phases should be the first-order transition. Across the Mott border at $P_c = 0.7 \text{ GPa}$, the system becomes a 2D Fermi liquid in the low-temperature region, which gradually extends at higher pressures. The suppression of the critical end point of the first-order Mott transition can arise from quantum fluctuations for a 2D triangular lattice system [4,5,31,32]. In general, the slope of the phase boundary dT_{MI}/dP is governed by the entropy difference between the insulating and metallic phases. The negative slope implies the presence of spin fluctuations and long-range ordering that reduce the insulating phase entropy. However, it is unlikely that spin fluctuations develop from such high temperatures towards the antiferromagnetic ordering at $T_{\text{N}} = 18 \text{ K}$. Indeed, the EtMe_3Sb salt without long-range ordering has a similar phase diagram [33]. Considering the system is located close to a charge order phase [21], the negative slope from high temperatures implies significant charge/orbital fluctuations in the insulating phase, otherwise the slope should be positive as observed in κ -(ET) $_2\text{Cu}_2(\text{CN})_3$ [34] and EtMe_3P at high temperatures [19].

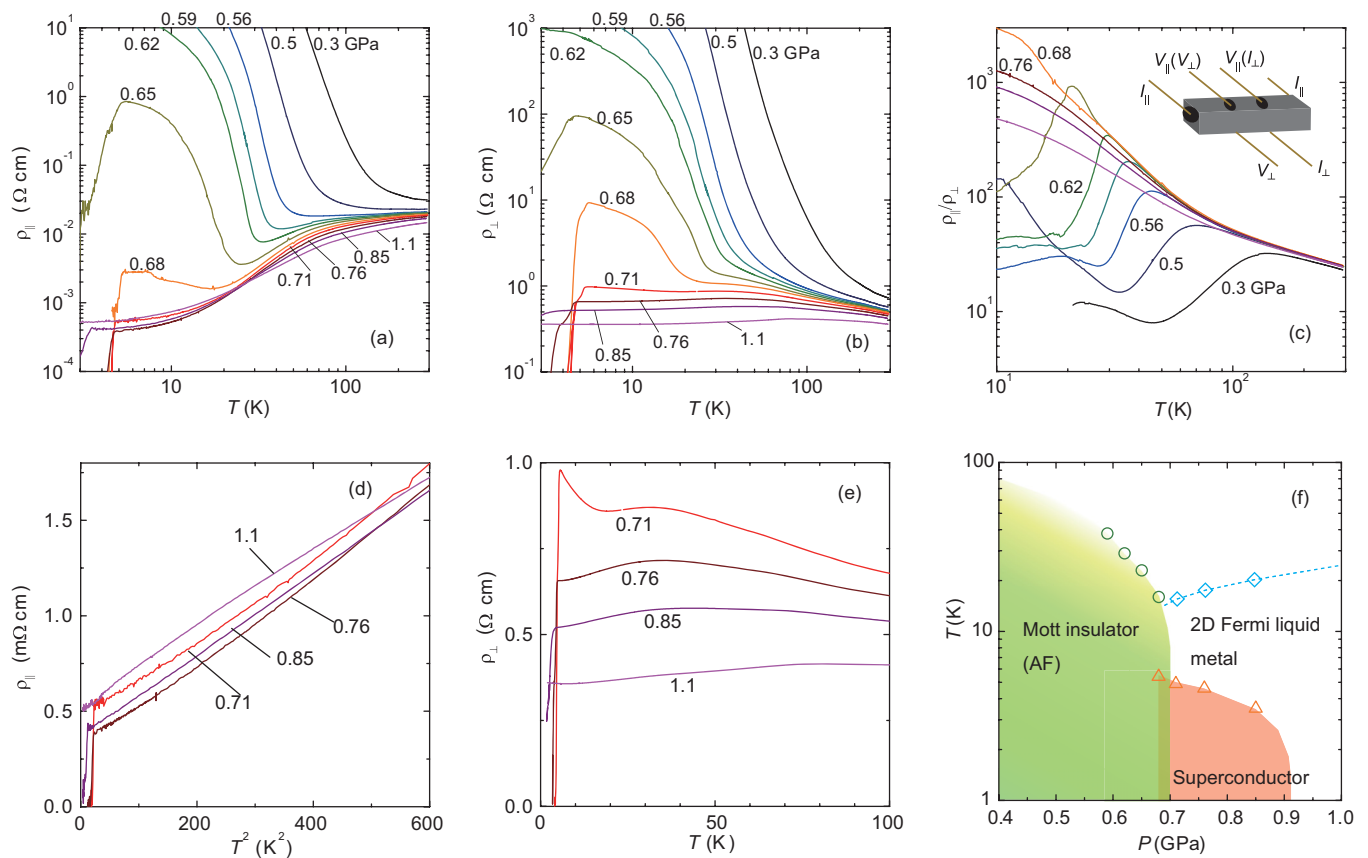


FIG. 2. Temperature dependence of (a) in-plane resistivity ρ_{\parallel} and (b) out-of-plane resistivity ρ_{\perp} of β' - $\text{Et}_2\text{Me}_2\text{As}[\text{Pd}(\text{dmit})_2]_2$ under hydrostatic pressures. (c) Resistivity anisotropy $\rho_{\perp}/\rho_{\parallel}$. Inset shows the contact arrangement of the six-probe measurement. (d) T^2 dependence of in-plane ρ_{\parallel} . (e) ρ_{\perp} at low temperatures and high pressures. (f) Pressure-temperature phase diagram based on the resistivity measurements in β' - $\text{Et}_2\text{Me}_2\text{As}[\text{Pd}(\text{dmit})_2]_2$, where the metal-insulator transition temperature (open circles) is defined by the resistivity minimum. The superconducting transition temperature (triangles) is defined by the onset of the resistivity drop. Open diamonds denote the onset temperature for the T^2 dependence of ρ_{\parallel} .

B. β - $\text{Me}_4\text{N}[\text{Pd}(\text{dmit})_2]_2$

The profile of ρ_{\parallel} for Me_4N behaves similar to $\text{Et}_2\text{Me}_2\text{As}$ under hydrostatic pressures, as shown in Fig. 3. The activation gap is obtained as 39 meV at 100 K and 0.3 GPa. Above 0.45 GPa, a metallic state is stabilized from high temperatures [Fig. 3(a)]. We obtained T_{MI} from the ρ_{\parallel} upturn (e.g., 40 K at 0.45 GPa) lowers with increasing pressure and is abruptly suppressed toward $P_c \sim 0.6$ GPa, above which the system becomes totally metallic. The superconducting transition is observed at $T_c = 6.5$ K for 0.54 GPa, which is still broad because of the fractional superconducting volume. A bulk superconducting transition appears above P_c and is suppressed at higher pressures. In contrast to $\text{Et}_2\text{Me}_2\text{As}$, a hump-like anomaly appears near 70 K, and it is less sensitive to pressure.

The behavior of ρ_{\perp} is remarkably different from that of ρ_{\parallel} . ρ_{\perp} is enhanced by an order of magnitude across 70 K [Fig. 3(b)]. It points to the reduction of the interlayer transfer via a structural distortion at the transition temperature $T_{\text{st}} = 70$ K. The transition becomes sharp and T_{st} gradually elevates with increasing pressure. As a result, $\rho_{\perp}/\rho_{\parallel}$ increases by an order of magnitude [Fig. 3(c)]. At low temperatures, however, ρ_{\perp} becomes metallic as observed in ρ_{\parallel} , which keeps $\rho_{\perp}/\rho_{\parallel} = 3\text{--}6 \times 10^2$. Because we observed no structural transition at ambient pressure, T_{st} must be present only under pressure.

A possible origin of the transition is the emergence of two inequivalent $\text{Pd}(\text{dmit})_2$ layers, as observed in $\text{Et}_2\text{Me}_2\text{P}$ under pressure [35] and α - Me_4N at ambient pressure [36] where one of the two layers involves charge ordering [36]. Kobayashi *et al.* also observed an anomaly at T_{st} , which showed strong sample dependence [23]. Our results of the resistivity anisotropy suggest that sample dependence arises from a different contact arrangement. Indeed, we confirmed no sample dependence on the ρ_{\parallel} and ρ_{\perp} measurements.

The T^2 dependencies of ρ_{\parallel} and ρ_{\perp} are plotted for the metallic state below 33 K in Figs. 3(d) and 3(e), respectively. We found good linearity in both ρ_{\parallel} and ρ_{\perp} for $T < 25\text{--}35$ K, indicating a Fermi liquid metal with a weak interlayer coherence. With increasing pressure, A_{\parallel} is suppressed away from the Mott boundary: A_{\parallel} changes from 4.2 to 2.0 $\mu\Omega\text{cm}/\text{K}^2$ from 0.61 to 1.1 GPa. Simultaneously, ρ_0 is suppressed from 0.85 to 0.40 m Ωcm . For ρ_{\perp} , we obtained $A_{\perp} = 730 \mu\Omega\text{cm}/\text{K}^2$ at 0.61 GPa, which is suppressed with increasing pressure.

The phase diagram of Me_4N [Fig. 3(f)] resembles that of $\text{Et}_2\text{Me}_2\text{As}$ except for the structural transition at $T_{\text{st}} = 65\text{--}75$ K. The phase boundary between the insulating and superconducting phases should be first order because the insulating phase has antiferromagnetic order. Across the Mott transition, the metallic state becomes a quasi-2D Fermi liquid metal, and

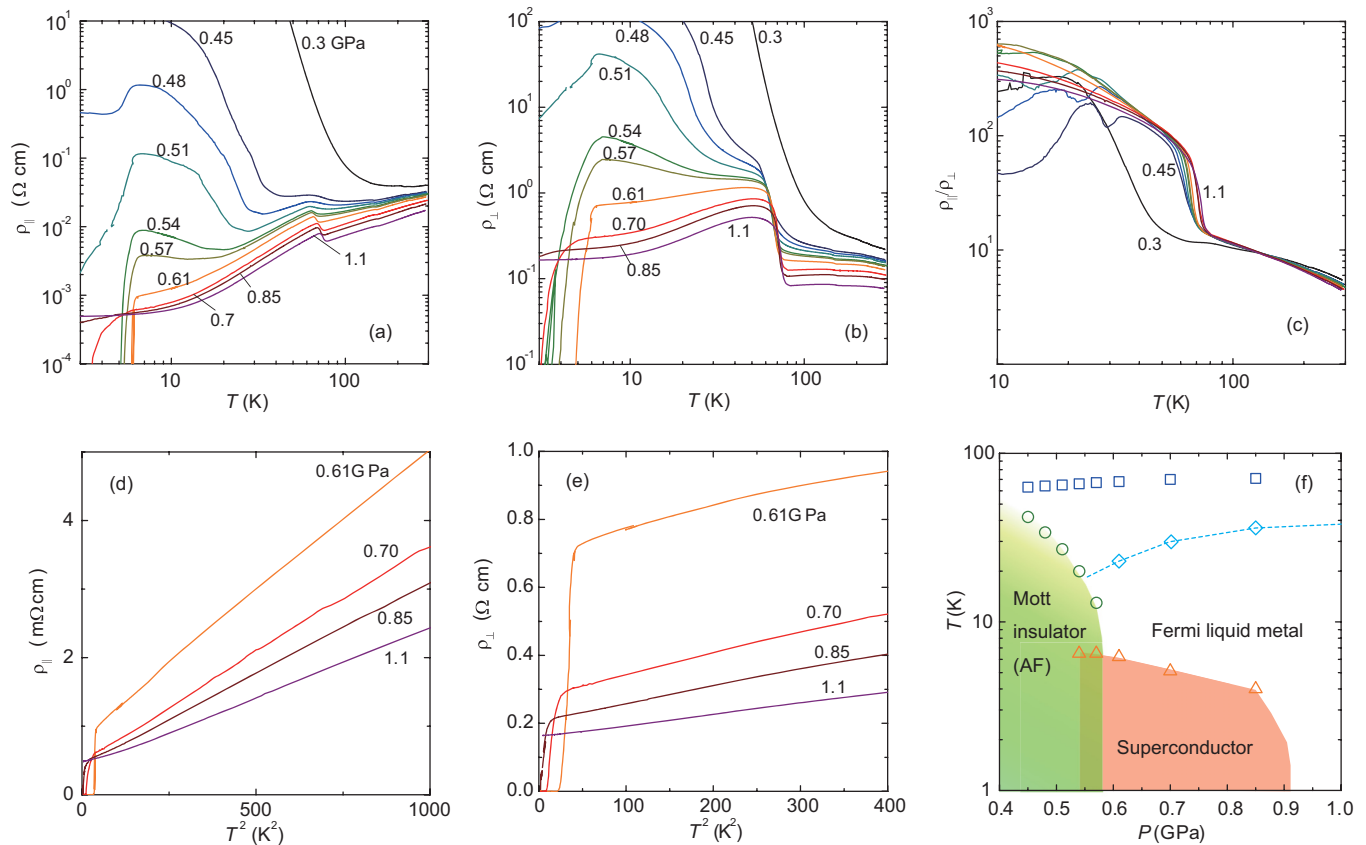


FIG. 3. Temperature dependence of (a) in-plane resistivity ρ_{\parallel} , (b) out-of-plane resistivity ρ_{\perp} , and (c) resistivity anisotropy $\rho_{\perp}/\rho_{\parallel}$ in $\beta\text{-Me}_4\text{N}[\text{Pd}(\text{dmit})_2]_2$. T^2 dependence of (d) ρ_{\parallel} and (e) ρ_{\perp} in the metallic state at low temperatures. (f) Pressure-temperature phase diagram of $\beta\text{-Me}_4\text{N}[\text{Pd}(\text{dmit})_2]_2$ based on the resistivity measurements. The open circles represent the metal-insulator crossover or transition defined by the resistivity minimum. The open squares denote the structural transition that changes the interlayer transfers. The insulating phase involves antiferromagnetic (AF) order below 12 K at ambient pressure, which is expected to suppress toward T_c under pressure. Open diamonds denote the onset temperature for the T^2 dependence of ρ_{\parallel} .

the region extends at higher pressures. Although a similar diagram of Me_4N was reported by Kobayashi *et al.* [23], they incorrectly interpreted the insulating phase as a spin-density wave state. If the charge order exists in one of the two layers below T_{st} , the negative slope of the phase boundary is naturally explained by the lower entropy on the insulating phase. The microscopic evidence should be identified by further nuclear magnetic resonance (NMR) measurements under pressure.

C. $\text{EtMe}_3\text{P}[\text{Pd}(\text{dmit})_2]_2$

The phase diagram of EtMe_3P was investigated in detail by ρ_{\parallel} [26] and thermoelectric power measurements [37]. On the critical pressure of the Mott transition, $P_c \sim 0.4$ GPa, we observed the metal-insulator and reentrant metal-to-insulator transitions in ρ_{\parallel} [Fig. 4(a)], as observed in the previous sample [26]. The later involves a clear thermal hysteresis, indicating a structure transition due to the VBO formation which vanishes under a high magnetic field [26]. The reentrant phase disappears in a narrow pressure range, and the insulator-metal transition becomes crossover above 0.41 GPa. Remarkably, ρ_{\parallel} (< 0.1 m Ω cm below 30 K) is an order of magnitude smaller than that of the other two salts with 2D transport properties.

As shown in Fig. 4(b), the temperature dependence of ρ_{\perp} behaves similarly to that of ρ_{\parallel} in the measured pressure range.

Surprisingly, $\rho_{\perp}/\rho_{\parallel}$ is smaller than 5 in the metallic phase. With increasing pressure, $\rho_{\perp}/\rho_{\parallel}$ is further suppressed and close to unity at 1.0 GPa [Fig. 4(c)]. The data are reproduced for another sample within the difference by a factor of 2 ($\rho_{\perp}/\rho_{\parallel} < 4$ for 1.0 GPa). Therefore, the system is regarded as a 3D metal with the significant interlayer transfers. As a result, the electron scattering contributing to ρ_{\parallel} is strongly suppressed in EtMe_3P .

In the metallic state, ρ_{\parallel} and ρ_{\perp} do not follow the T^2 law but a relation $\rho_0 + AT^n$ ($n = 2.5$). As shown in Figs. 4(d) and 4(e), we find good linearity in both ρ_{\parallel} and ρ_{\perp} plotted against $T^{2.5}$ below 15 K. The behavior persists for an extensive pressure range, 0.5–1.0 GPa. Thus, the electron scattering mechanism in EtMe_3P differs from that of the correlated Fermi liquid. The power $n > 2$ is typically observed in quasi-one-dimensional (1D) systems such as Nb_2Se_3 [38], $(\text{DI-DCNQI})_2\text{Ag}$ [39], and KRu_4O_8 , [40], where higher-order Umklapp scattering due to charge density waves is dominant in the resistivity [41]. In the present case, the insulating phase has VBO, where the localized spin $S = 1/2$ is dimerized by the lattice distortion along the molecular column. As shown in the P - T phase diagram [Fig. 4(f)], the VBO phase persists until the Mott transition terminates, where the VBO transition is determined by the maximum of the charge gap and the reentrant Mott transition [26]. In the 3D metallic phase, the temperature

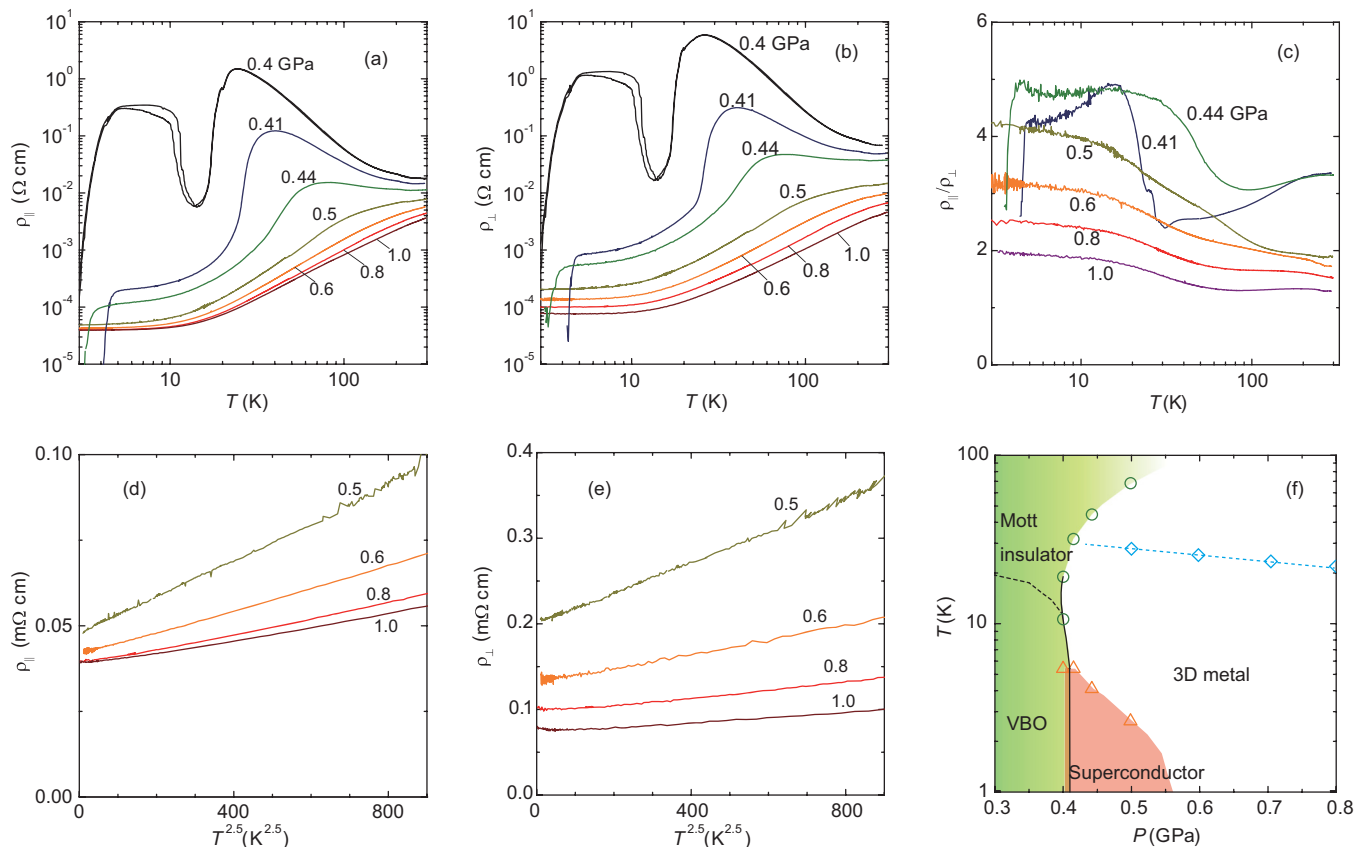


FIG. 4. Temperature dependence of (a) in-plane resistivity ρ_{\parallel} , (b) out-of-plane resistivity ρ_{\perp} , and (c) resistivity anisotropy $\rho_{\perp}/\rho_{\parallel}$ in $\text{EtMe}_3\text{P}[\text{Pd}(\text{dmit})_2]_2$. $T^{2.5}$ dependence of (d) ρ_{\parallel} and (e) ρ_{\perp} . (f) Pressure-temperature phase diagram of $\text{EtMe}_3\text{P}[\text{Pd}(\text{dmit})_2]_2$. The dotted line in the insulating phase represents the valence bond order (VBO) transition showing the maximum activation gap in resistivity and the solid line represents the first-order Mott transition [26]. The insulator-metal transition temperature is defined as the resistivity inflection. Open diamonds denote the onset temperature for the $T^{2.5}$ dependence of ρ_{\parallel} .

range showing the $T^{2.5}$ resistivity narrows away from the Mott border. The significant higher-order Umklapp scattering in the metallic state suggests that the VBO fluctuations due to strong electron-phonon coupling can be highlighted owing to the depressed electron-electron scattering for the 3D coherency.

IV. DISCUSSION

We show the characteristic in-plane and out-of-plane resistivity data across the Mott transition for the three types of $\text{Pd}(\text{dmit})_2$ compounds with different molecular packing. The β' -type $\text{Et}_2\text{Me}_2\text{As}$ salt has the largest resistivity anisotropy $\rho_{\perp}/\rho_{\parallel}$ exceeding 10^3 and the semiconducting ρ_{\perp} , featuring incoherent interlayer transport as observed in the high- T_c cuprates [42–44]. The β -type Me_4N salt also shows the high anisotropy $\rho_{\perp}/\rho_{\parallel} \sim 300$, while ρ_{\perp} is metallic at low temperatures. In stark contrast, the EtMe_3P salt exhibits a nearly isotropic metallic state. To gain insight into the difference of the electronic state, we evaluate the bond length and the interlayer transfer integral for the crystal structure at ambient pressure. We find that the shortest interlayer S-S distances between $\text{Pd}(\text{dmit})_2$ molecules are 5.31 Å for $\text{Et}_2\text{Me}_2\text{As}$, 4.46 Å for Me_4N , and 3.68 Å for EtMe_3P at 300 K. This order is different from that of the cation size, $\text{Me}_4\text{N} < \text{EtMe}_3\text{P} < \text{Et}_2\text{Me}_2\text{As}$. Hence, the S-S contact strongly depends on the

type of molecular packing and the cation location. Because the intermolecular distances are expected to shorten under hydrostatic pressure, the interlayer S-S distance of EtMe_3P can be even shorter than the Van der Waals distance 3.6 Å at high pressures, consistent with the coherent interlayer transport.

The interlayer transfer integrals between $\text{Pd}(\text{dmit})_2$ molecules t_{\perp} are calculated with the extended Hückel method. We obtain t_{\perp} as 1.4, 0.16, and 0.01 meV for EtMe_3P , Me_4N , and $\text{Et}_2\text{Me}_2\text{As}$, respectively, consistent with the order of the interlayer S-S distance. Remarkably, t_{\perp} of EtMe_3P is two orders of magnitude greater than that of $\text{Et}_2\text{Me}_2\text{As}$. Such a large t_{\perp} is unique to the $\text{Pd}(\text{dmit})_2$ salt having terminal S atoms with the sizable electron density near the Fermi level and explains the 3D transport property. In the well-known quasi-2D system $\kappa\text{-(ET)}_2\text{Cu}(\text{NCS})_2$ with interlayer coherency [12], t_{\perp} is experimentally evaluated as 0.065 meV [45], which is lower than Me_4N and higher than $\text{Et}_2\text{Me}_2\text{As}$. The cutoff t_{\perp} for the coherent transport can be located between them.

For ideal 2D systems with triangular lattices, the critical point is suppressed to low temperatures owing to quantum fluctuations [4,5,31,32]. In a critical region, the resistivity is predicted to approach the T -invariant universal resistance $\rho_b = \hbar/e^2 \times R = 205 \text{ k}\Omega$, $R = 49.8$ [32]. Indeed we find that ρ_{\parallel} of $\text{Et}_2\text{Me}_2\text{As}$ becomes nearly independent of temperature above 100 K around P_c . The saturated value $\rho_{\parallel} \sim 0.015 \text{ }\Omega\text{cm}$

gives the sheet resistance $\rho_{||}/d = 0.5 \times 10^5 \Omega$ for the sample thickness $d = 0.03$ mm, in agreement with the order of the universal resistance. For the determination of the critical exponents, more accurate pressure control is required on isothermal measurements. As for EtMe₃P, the Mott transition is recently interpreted as 2D Ising universality [37]. Our results demonstrating the 3D transport property suggest the reconsideration for universality.

Finally, we remark on the common feature on the P - T phase diagram for the three compounds. We find that the superconducting phases ($T_c = 5$ – 7 K) commonly emerge from Mott insulating phases with different magnetic ground states and are suppressed away from the Mott border. It might indicate a significant role of electron correlations in the emergence of superconductivity. The electron-electron interaction is highlighted for the quasi-2D compounds with the neighboring antiferromagnetic insulator phase. Further systematic studies on the β' salts as a function of t'/t will clarify the effect of spin fluctuations in unconventional superconductivity. In this respect, the superconductivity on EtMe₃P is quite unusual because the electron correlation is strongly suppressed in the metallic phase. Rather, the electron-phonon coupling may be important for driving Cooper pairing, as is known in conventional superconductors. Our results pose a fundamental question that the superconductivity appearing near the Mott transition is not necessarily related to electron correlations.

V. CONCLUSION

The resistivity anisotropy on the molecular Mott insulators $Z[\text{Pd}(\text{dmit})_2]_2$ demonstrated contrasting interlayer transport properties depending on intermolecular interactions. We find that the antiferromagnetic Mott insulator β' -Et₂Me₂As[Pd(dmit)₂]₂ is an ideal 2D system of Mott transition into a Fermi liquid metal with incoherent interlayer resistivity. In β -Me₄N[Pd(dmit)₂]₂, the dimensionality changes across the structural transition, where two Pd(dmit)₂ layers may become inequivalent. Strong electron correlations are manifested as the T^2 resistivity for these 2D compounds. In contrast, the nearly isotropic metal is realized in EtMe₃P[Pd(dmit)₂]₂ through the sizable interlayer transfers. As a result, the electron-electron scattering is depressed in the metallic state. Instead, the electron-phonon coupling is highlighted because of the presence of the valence bond order in the neighboring Mott insulating phase. Such a variety of dimensionality in $Z[\text{Pd}(\text{dmit})_2]_2$ is inherent to the high electron density of the terminal S atoms in the Pd(dmit)₂ molecule. The series of materials provides a significant platform for investigating the effect of dimensionality on Mott-Hubbard systems.

ACKNOWLEDGMENTS

This work was supported by MEXT/JSPS KAKENHI Grants (No. JP16GS0219, No. JP16H06346, and No. JP17H05151).

-
- [1] A. Georges, G. Kotliar, W. Krauth, and M. J. Rozenberg, *Rev. Mod. Phys.* **68**, 13 (1996).
 - [2] P. W. Anderson and Z. Zou, *Phys. Rev. Lett.* **60**, 132 (1988).
 - [3] T. Senthil, *Phys. Rev. B* **78**, 045109 (2008).
 - [4] T. Valla, P. D. Johnson, Z. Yusof, B. Wells, Q. Li, S. M. Loureiro, R. J. Cava, M. Mikami, Y. Mori, M. Yoshimura, and T. Sasaki, *Nature (London)* **417**, 627 (2002).
 - [5] R. V. Mishmash, I. Gonzalez, R. G. Melko, O. I. Motrunich, and M. P. A. Fisher, *Phys. Rev. B* **91**, 235140 (2015).
 - [6] L. Zou and T. Senthil, *Phys. Rev. B* **94**, 115113 (2016).
 - [7] A. Ardavan, S. Brown, S. Kagoshima, K. Kanoda, K. Kuroki, H. Mori, M. Ogata, S. Uji, and J. Wosnitza, *J. Phys. Soc. Jpn.* **81**, 011004 (2012).
 - [8] K. Kanoda and R. Kato, *Annu. Rev. Condens. Matter Phys.* **2**, 167 (2011).
 - [9] Y. Shimizu, K. Miyagawa, K. Kanoda, M. Maesato, and G. Saito, *Phys. Rev. Lett.* **91**, 107001 (2003).
 - [10] P. Limelette, P. Wzietek, S. Florens, A. Georges, T. A. Costi, C. Pasquier, D. Jérôme, C. Mézière, and P. Batail, *Phys. Rev. Lett.* **91**, 016401 (2003).
 - [11] F. Kagawa, K. Miyagawa, and K. Kanoda, *Nature (London)* **436**, 534 (2005).
 - [12] J. Singleton, P. A. Goddard, A. Ardavan, A. I. Coldea, S. J. Blundell, R. D. McDonald, S. Tozer, and J. A. Schlueter, *Phys. Rev. Lett.* **99**, 027004 (2007).
 - [13] R. H. McKenzie and P. Moses, *Phys. Rev. Lett.* **81**, 4492 (1998).
 - [14] R. Kato, *Bull. Chem. Soc. Jpn.* **87**, 355 (2014).
 - [15] R. Kato and C. Hengbo, *Crystals* **2**, 861 (2012).
 - [16] T. Tsumuraya, H. Seo, M. Tsuchiizu, R. Kato, and T. Miyazaki, *J. Phys. Soc. Jpn.* **82**, 033709 (2013).
 - [17] T. Nakamura, T. Takahashi, S. Aonuma, and R. Kato, *J. Mater. Chem.* **11**, 2159 (2001).
 - [18] M. Tamura and R. Kato, *J. Phys.: Condens. Matter* **14**, L729 (2002).
 - [19] Y. Shimizu, H. Akimoto, H. Tsujii, A. Tajima, and R. Kato, *J. Phys.: Condens. Matter* **19**, 145240 (2007).
 - [20] T. Itou, A. Oyamada, S. Maegawa, and R. Kato, *Nat. Phys.* **6**, 673 (2010).
 - [21] T. Yamamoto, M. Tamura, K. Yakushi, and R. Kato, *J. Phys. Soc. Jpn.* **85**, 104711 (2016).
 - [22] M. Tamura, A. Nakao, and R. Kato, *J. Phys. Soc. Jpn.* **75**, 093701 (2006).
 - [23] A. Kobayashi, A. Miyamoto, R. Kato, A. Sato, and H. Kobayashi, *Bull. Chem. Soc. Jpn.* **71**, 997 (1998).
 - [24] R. Kato, A. Tajima, A. Nakao, and M. Tamura, *J. Am. Chem. Soc.* **128**, 10016 (2006).
 - [25] T. Yamamoto, Y. Nakazawa, M. Tamura, A. Nakao, A. Fukaya, R. Kato, and K. Yakushi, *J. Phys. Soc. Jpn.* **83**, 053703 (2014).
 - [26] Y. Shimizu, H. Akimoto, H. Tsujii, A. Tajima, and R. Kato, *Phys. Rev. Lett.* **99**, 256403 (2007).
 - [27] K. Murata, H. Yoshino, H. Om Yadav, Y. Honda, and N. Shirakawa, *Rev. Sci. Instrum.* **68**, 2490 (1997).
 - [28] N. F. Mott, *Metal-Insulator Transition*, edited by T. Francis, (Taylor & Francis, London, 1990).

- [29] A. C. Jacko, J. O. Fjarestad, and B. J. Powell, *Nat. Phys.* **5**, 422 (2009).
- [30] R. Busch, G. Ries, H. Werthner, G. Kreiselmeyer, and G. Saemann-Ischenko, *Phys. Rev. Lett.* **69**, 522 (1992).
- [31] M. Imada, *J. Phys. Soc. Jpn.* **73**, 1851 (2004).
- [32] W. Witczak-Krempa, P. Ghaemi, T. Senthil, and Y. B. Kim, *Phys. Rev. B* **86**, 245102 (2012).
- [33] T. Furukawa, K. Miyagawa, H. Taniguchi, R. Kato, and K. Kanoda, *Nat. Phys.* **11**, 221 (2015).
- [34] Y. Kurosaki, Y. Shimizu, K. Miyagawa, K. Kanoda, and G. Saito, *Phys. Rev. Lett.* **95**, 177001 (2005).
- [35] J. Yamaura, A. Nakao, and R. Kato, *J. Phys. Soc. Jpn.* **73**, 976 (2004).
- [36] R. Kato *et al.* (unpublished).
- [37] M. Abdel-Jawad, R. Kato, I. Watanabe, N. Tajima, and Y. Ishii, *Phys. Rev. Lett.* **114**, 106401 (2015).
- [38] M. H. Rashid and D. J. Sellmyer, *Phys. Rev. B* **29**, 2359 (1984).
- [39] T. Itou, K. Kanoda, K. Murata, T. Matsumoto, K. Hiraki, and T. Takahashi, *Phys. Rev. Lett.* **93**, 216408 (2004).
- [40] W. Kobayashi, *Phys. Rev. B* **79**, 155116 (2009).
- [41] A. Oshiyama, K. Nakao, and H. Kamimura, *J. Phys. Soc. Jpn.* **45**, 1136 (1978).
- [42] S. Martin, A. T. Fiory, R. M. Fleming, L. F. Schneemeyer, and J. V. Waszczak, *Phys. Rev. B* **41**, 846 (1990).
- [43] Y. Ando, G. S. Boebinger, A. Passner, N. L. Wang, C. Geibel, and F. Steglich, *Phys. Rev. Lett.* **77**, 2065 (1996).
- [44] T. Watanabe, T. Fujii, and A. Matsuda, *Phys. Rev. Lett.* **79**, 2113 (1997).
- [45] P. A. Goddard, S. J. Blundell, J. Singleton, R. D. McDonald, A. Ardavan, A. Narduzzo, J. A. Schlueter, A. M. Kini, and T. Sasaki, *Phys. Rev. B* **69**, 174509 (2004).